



## Dual template using P123-gelatin for synthesized large mesoporous silica for enhanced adsorption of dyes

Widiya Nur Safitri<sup>a</sup>, Habiddin Habiddin<sup>a</sup>, Maria Ulfa<sup>b</sup>, Wega Trisunaryanti<sup>c</sup>, Hasliza Bahruji<sup>d</sup>, Holilah Holilah<sup>a,e,f</sup>, Alya Awinatul Rohmah<sup>a</sup>, Novia Amalia Sholeha<sup>g</sup>, Aishah Abdul Jalil<sup>h</sup>, Eko Santoso<sup>a</sup>, Didik Prasetyoko<sup>a,\*</sup>

<sup>a</sup> Department of Chemistry, Faculty of Science and Data Analytics, Institut Teknologi Sepuluh Nopember, Keputih, Sukolilo, Surabaya 60111, East Java, Indonesia

<sup>b</sup> Chemistry Education Study Program, Faculty of Teacher Training and Education, Universitas Sebelas Maret, Jl. Ir. Sutani 36A, Surakarta 57126, Central Java Indonesia

<sup>c</sup> Department of Chemistry, Faculty of Science, Universitas Gadjah Mada, Sekip Utara Sleman, Indonesia

<sup>d</sup> Centre for Advanced Material and Energy Sciences, Universiti Brunei Darussalam, Bandar Seri Begawan BE 1410, Brunei Darussalam

<sup>e</sup> Research Center for Biomass and Bioproducts, National Research and Innovation Agency of Indonesia (BRIN), Cibinong 16911, Indonesia

<sup>f</sup> Department of Food Science and Technology, Faculty of Agriculture, Halu Oleo University, Indonesia

<sup>g</sup> College of Vocational Studies, Bogor Agricultural University (IPB University), Jalan Kumpang No. 14, Bogor 16151, Indonesia

<sup>h</sup> Department of Chemical Engineering, Faculty of Chemical and Energy Engineering, Universiti Teknologi Malaysia, 81310 UTM, Skudai, Johor Bahru, Johor, Malaysia

### ARTICLE INFO

#### Keywords:

Mesoporous silica  
Gelatin  
Dual template  
Pluronic P123  
Dye

### ABSTRACT

Mesoporous Silica with a large mesopore channel was synthesized using the sol-gel method for dye adsorption. A dual template consisting of P123 and gelatin at different ratios was employed in the sol-gel synthesis to enhance surface area and mesopore diameter. Gelatin is a green pore directing agent that strengthens P123 thermal stability during the calcination of silicate gel. Optimization of P123:gelatin ratio to 1:0.02 increased the surface area of mesoporous silica to 561.9 m<sup>2</sup>/g and expanded the pore diameter to 10 nm. The large pore diameter and surface area enhanced methylene blue adsorption capacity to 363.63 mg/g. The adsorption of methylene blue on mesoporous silica follows the pseudo second-order kinetic and the Langmuir model. Regeneration studies using thermal and chemical treatments exhibited the potential of mesoporous silica as an adsorbent for multiple adsorption-desorption of dyes.

### 1. Introduction

Water pollution from untreated dyes has become a severe global issue that requires immediate attention (Karthik et al., 2015). Methylene blue (MB) is an azo heterocyclic dye used in the textile industry with carcinogenic, mutagenic, and toxic properties (Xue et al., 2022). Methylene blue removal in wastewater has been widely investigated via bioremediation (Upendar et al., 2017), ozonation and chlorination, coagulation, and adsorption (Etchepare et al., 2015). Methylene blue removal via adsorption is a low-cost, practical, straightforward process (Karthik et al., 2015; Rafatullah et al., 2010). Activated carbon and zeolite are two materials commonly utilized for dye adsorption, with the modification of pore size and structure being actively investigated to enhance the adsorption capacity (Li and Wu, 2009). Mesoporous silica exhibited a high adsorption capacity due to its large pore structure

(4.6–30 nm) to allow diffusion of large structure dye, thick pore walls that are stable during regeneration of adsorbent, and uniform size with high surface area for large adsorption capacity (Albayati et al., 2019; Chen et al., 2017; Sari Yilmaz, 2022). Mesoporous silica as methylene blue adsorbent provides monolayer adsorption with 192 mg/g adsorption capacity (Han et al., 2021).

Sol-gel is a standard method for synthesizing mesoporous silica (Zhang et al., 2009; Rehman et al., 2014). Surfactant is used in sol-gel synthesis to improve uniformity, increase the surface area, and produce homogeneous pores through the formation of micelles (Wüstneck and Kragel, 1998) (Karakiliç et al., 2019) (Xie et al., 2016). Synthetic surfactants is seen as non-environmental friendly because of the difficulty of degrading by nature. As a template, it has a low affinity due to the lack of attracting groups (Rajendhiran et al., 2021), and low mechanical stability, particularly at high temperatures (He and

\* Corresponding author.

E-mail address: [didikp@chem.its.ac.id](mailto:didikp@chem.its.ac.id) (D. Prasetyoko).

<https://doi.org/10.1016/j.sajce.2022.11.011>

Received 15 August 2022; Received in revised form 25 October 2022; Accepted 23 November 2022

Available online 25 November 2022

1026-9185/© 2022 The Authors. Published by Elsevier B.V. on behalf of South African Institution of Chemical Engineers. This is an open access article under the CC BY-NC-ND license (<http://creativecommons.org/licenses/by-nc-nd/4.0/>).

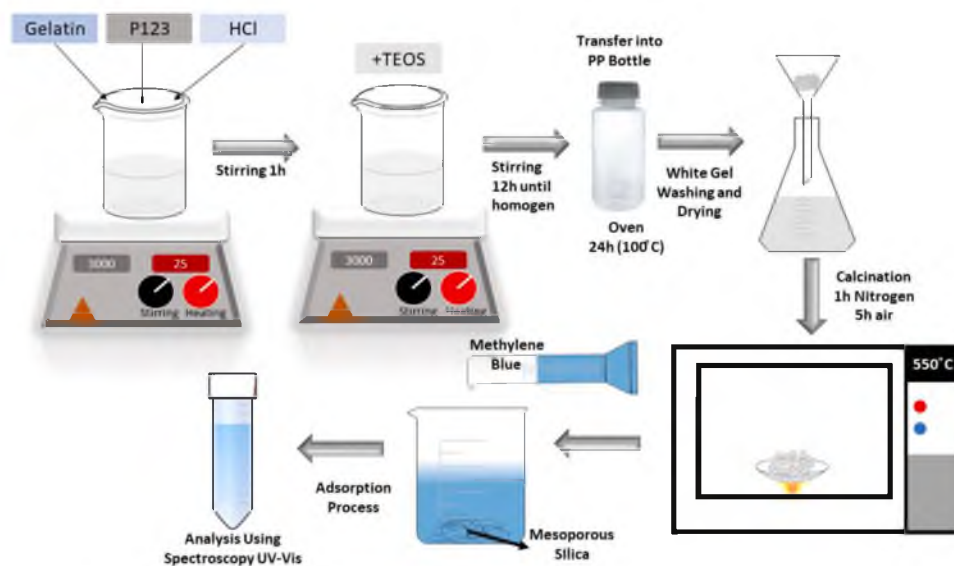


Fig. 1. Schematic diagram to illustrate the synthesis of mesoporous silica and the adsorption studies.

Alexandridis, 2018). Gelatin, gum Arabic, and starch are three naturally occurring pore-directing templates utilized for synthesizing mesoporous materials (Ulfa et al., 2020; Tako et al., 2014). A low concentration of gelatin is required to form a high surface area and porous hexagonal flake-like hematite ( $\alpha\text{-Fe}_2\text{O}_3$ ) and carbon microsphere (MCMs) (Ulfa et al., 2020; Ulfa et al., 2021). Gelatin also acts as a structure-directing agent to develop various morphological structures such as microspheres, wormhole-like, and sponge-shaped carbon (Ulfa et al., 2020; Ulfa et al., 2018).

Despite its potential prospect as a green template, gelatin is unstable for high temperature synthesis and often produces materials with low porosity (Veisi et al., 2020). This problem can be solved using a hybrid template combining gelatin with synthetic surfactant. The hybrid template minimizes synthetic surfactant usage and improves template stability during high temperature synthesis. Our previous studies showed that hybrid gelatin with F127 produced a high surface area of silica and formed uniform carbon microspheres with high thermal stability (Ulfa et al., 2018). This study will employ a soft template of triblock copolymer P123 with gelatin to synthesize large mesoporous silica. P123 is widely used to form SBA-15 with regular hexagonal pores of 104–320 Å with wide spacing distances and high surface area of 69–104 m<sup>2</sup> (Postnova et al., 2017). The composition of P123 directly affects the resulting morphology, in which a low P123 concentration forms a cubic structure, while the excess P123 concentration produces a mesoporous lamellar structure (Kumar et al., 2017). Based on a high electrostatic interaction between gelatin and silica through N–H functional group and silanol groups (Si–OH), the combination with P123 further enhanced the efficiency of producing materials with enhanced physicochemical properties (Coradin et al., 2004; Sachithanadam and Joshi, 2014). This study will determine the effect of a high concentration of gelatin as a co-template for P123, on expanding the mesopore size and surface area of silica. The surface area and porosity effect will be evaluated as an adsorbent for methylene blue removal.

## 2. Experimental

### 2.1. Materials

Gelatin ( $\text{C}_{102}\text{H}_{151}\text{N}_{31}\text{O}_{39}$ ,  $\geq 99\%$ , Sigma Aldrich, Europe), Triblock Copolymer (P123) ( $\text{HO}(\text{CH}_2\text{CH}_2\text{O})_{20}(\text{CH}_2\text{CH}(\text{CH}_3)\text{O})_{70}(\text{CH}_2\text{CH}_2\text{O})_{20}\text{H}$ , Sigma-Aldrich, Pte. Ltd), Tetraethyl orthosilicate ( $\text{Si}(\text{OC}_2\text{H}_5)_4$ , 98%, Sigma-Aldrich, Pte. Ltd), Hydrochloride (HCl, 37%, Merck, US-Canada),

Methanol ( $\text{CH}_3\text{OH}$ ,  $\geq 99.9\%$ , Merck, Amerika), Acetone ( $\text{C}_3\text{H}_6\text{O}$ ,  $\geq 99.5\%$ , Merck, Amerika), Aquades ( $\text{H}_2\text{O}$ , 99%, Nirwana, Surabaya), Methylene Blue ( $\text{C}_{16}\text{H}_{18}\text{ClN}_3\text{S} \times \text{H}_2\text{O}$ , Merck, ACS, Reag. pH Eur, Amerika), Methyl Orange ( $\text{C}_{14}\text{H}_{14}\text{N}_3\text{NaO}_3\text{S}$ , Reag. pH Eur, Merck, Amerika), Malachite Green ( $\text{C}_{48}\text{H}_{50}\text{N}_4\cdot 2\text{C}_2\text{H}_2\text{O}_4\cdot \text{C}_2\text{H}_2\text{O}_4$ , Reag. pH Eur, Merck, Amerika), and Congo Red ( $\text{C}_{32}\text{H}_{22}\text{N}_6\text{Na}_2\text{O}_6\text{S}_2$ , Reag. pH Eur, Merck, Amerika).

### 2.2. Synthesis mesoporous silica

Mesoporous silica was synthesized using the sol-gel method by dissolving P123 into 150 mL of HCl 2 M. Gelatin was added at different concentrations of 0.2, 0.5, and 1 wt% and stirred for 1 hour. After 1 hour, 11 mL TEOS was added, and the mixture was stirred for 12 h. The mixture was placed in a polypropylene bottle and heated at 100 °C for 24 h. The solid was filtered using distilled water until the pH of the supernatant was neutral to remove the impurities. The solid was dried and calcined at 550 °C for 6 h in a furnace at 2 °C/min ramp rate. The schematic diagram for all the processes is shown in Fig. 1. The resulting silica were labelled based on the ratio between P123:gelatin (MS = 1:0; MS-0.2 = 1:0.2, MS-0.5 = 1:0.5; and MS-1 = 1:1).

### 2.3. Characterization of the material

Mesoporous silica samples were characterized by X-ray diffraction (XRD, PANalytical X'pert Pro, US) with Cu K $\alpha$  radiation over  $2\theta$  ranging from 0° to 60° and  $\lambda=1.54056$ . The porosity and surface area were analyzed using N<sub>2</sub> physisorption at 77 K (Nova 1200 Quantachrome, Bel Inc., Japan). The sample (0.05 g) was degassed at 300 °C for 3 h prior to N<sub>2</sub> analysis. The surface area was calculated using Brunauer-Emmett-Teller (BET) method, and the pore size distribution was determined using the non-local density function theoretical method (NLDFT). Fourier Transform Infrared Spectroscopy (FTIR, SHIMADZU 96,500, Japan) spectra were recorded in the 4000–400 cm<sup>-1</sup> wavenumber. The morphology was determined using Scanning Electron Microscopy (SEM-EDX, JEOL 6360 LA, Japan) and Transmission Electron Microscopy (TEM, Hitachi HT7700, Japan). The particle size distribution was measured using image-J software based on the average of 30 measurements from the SEM images. Thermogravimetric analysis (TG) and Difference Thermo Gravimetric (DTG) were performed using Thermoanalyzer Setaram model LABSYS<sub>tm</sub>, Swedia from 25 to 600 °C at 10 °C min<sup>-1</sup> ramp rate. Zeta potential was measured by Zetasizer NanoZS,

Malvern, US, with a concentration of 0.01 g/ml. The concentration of the dyes during the adsorption study was analyzed using a SHIMADZU UV-26,001, Japan, spectrophotometer.

#### 2.4. Adsorption of methylene blue

Methylene blue stock solution (200 ppm) was prepared by dissolving 0.5 g of methylene blue powder in 250 mL of distilled water. The stock solution was diluted for the preparation of calibration solutions. The maximum wavelength of methylene blue was determined using a 10 ppm solution in a cuvette at a wavelength range of 400–800 nm. The calibration plot of methylene blue solution was determined using 1, 2, 3, 4, 5, and 6 ppm concentrations. Batch adsorption of methylene blue was carried out using 0.005 g of as-obtained porous material MS; MS-0.2; MS-0.5; and MS-1 with 15 mL of MB aqueous solutions in 50 mL glass flasks. The mixture was stirred at 200 rpm for 60 min at room temperature. The effect of the contact time on methylene blue removal was conducted at 2.5, 5, 10, 20, 30, and 60 min. The effect of adsorbent dosage was observed using 2.5, 5, 7.5, and 10 mg of mesoporous silica with the initial MB concentration of 30 mg/L. The effect of MB solution concentration was determined using 10, 30, 50, 70, 90, 110, 130, and 150 ppm. After the mixture was centrifuged for 5 min, the supernatant was separated from the adsorbent by centrifugation at 2000 rpm for 5 min. The concentration of MB supernatant was measured by UV–vis spectrophotometer at the 664 nm wavelength. The adsorption capacity ( $q_e$ , mg/g<sup>-1</sup>) and removal efficiency (%) of MB onto the porous materials were calculated by the following Eqs. (1)–(3):

$$q_e = \frac{(C_o - C_e)V}{W} \quad (1)$$

$$q_t = \frac{(C_o - C_t)V}{W} \quad (2)$$

$$\text{Removal (\%)} = \frac{(C_o - C_e)}{C_o} \times 100 \quad (3)$$

Where  $C_o$  is the initial concentration of MB in the solution;  $C_t$  and  $C_e$  represent the final dye concentrations (mg/L) at a given contact time ( $t$ ) and equilibrium, respectively;  $V$  is the volume of MB solution;  $W$  is the weight of the mesoporous silica; and  $q_e$  and  $q_t$  are the adsorption capacities per unit mass of mesoporous silica at equilibrium and at a given time ( $t$ ), respectively.

#### 2.5. Desorption study

##### 2.5.1. Using thermal and chemical regeneration method

Regeneration of MB from the adsorbent was performed using thermal and chemical regeneration methods. Thermal regeneration was carried out four times using MS-0.2. The silica that has been adsorbed with methylene blue is calcined at 550 °C for 3 h. After the calcination, the MS-0.2 material was reused for the adsorption process. In chemical regeneration of mesoporous silica, HCl, methanol, water, and acetone were used respectively as a solvent to remove adsorbed MB on MS-0.2. The silica was dispersed into solvents for 30 min, filtered and dried at 120 °C. The selection of solvents was based on the desorption efficiency of MB measured using a UV–vis spectrophotometer. The adsorption-desorption was repeated to determine the reusability of mesoporous silica. The desorption efficiency was calculated using Eq. (4) (Tehubijuluw et al., 2022)

$$\% \text{ Desorption Efficiency} = \frac{\text{Amount of dye desorbed from the adsorbent}}{\text{Amount of the adsorbed by the adsorbent}} \times 100 \quad (4)$$

The possibility of regeneration and reusability was also investigated by carrying out the adsorption-desorption process for four cycles using

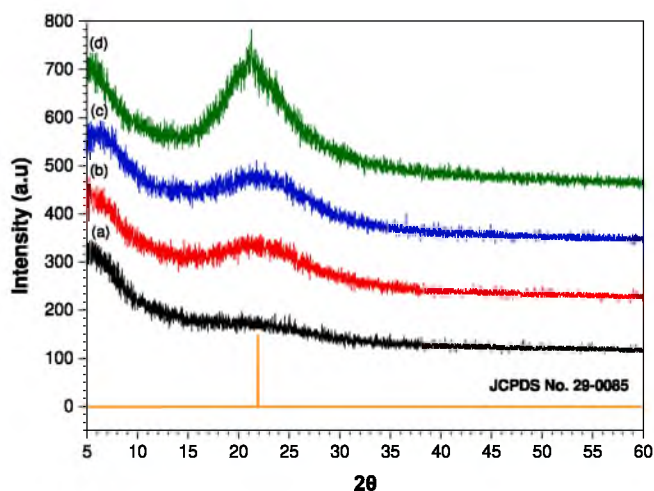


Fig. 2. XRD pattern of the sample mesoporous silica a. MS; b. MS-0.2; c. MS-0.5, d. MS-1.

acetone.

### 3. Results and discussion

#### 3.1. Catalyst preparation and characterization of mesoporous silica

Mesoporous silica was analyzed using XRD between  $2\theta = 5 - 60^\circ$  as shown in Fig. 2. The XRD showed a broad peak at  $2\theta = 21 - 25^\circ$ , which is a typical diffraction pattern of amorphous silica, according to JCPDS XRD standard No. 29-0085 (Dubey et al., 2015). Mesoporous silica produced using higher gelatin ratios showed a more intense peak but maintained a similar broad diffraction pattern. No other peaks were observed, indicating no impurities that may be resulted from the residual carbon. Gelatin increased the regularity of the amorphous structure due to its strong affinity when interacting with silica to direct it into a more regular amorphous structure (Mahony et al., 2014).

The textural properties of mesoporous silica were determined using N<sub>2</sub> adsorption-desorption analysis at 77 K. The N<sub>2</sub> adsorption-desorption isotherm in Fig. 3(a) showed the type IV adsorption isotherm for all samples with an H1 hysteresis loop according to the IUPAC classification (Rayati et al., 2018). The type IV isotherm is a characteristic of mesoporous material with a hexagonal pore arrangement. The mesoporous silica produced from a dual template shows a similar isotherm with loop hysteresis at a relatively high-pressure range ( $0.4 < P/P_0 < 0.8$ ). The hysteresis loop represents a spontaneous filling of mesopores due to capillary condensation (Barranco-García et al., 2018; Yuan et al., 2018). The calculated data based on the N<sub>2</sub> adsorption-desorption isotherm is shown in Table 1. MS with the highest surface area was obtained using 0.2% gelatin, which was 561.9 m<sup>2</sup>/g. The surface area was significantly increased compared to MS obtained from P123 only at 482 m<sup>2</sup>/g. However, when the ratio was further increased to 0.5 and 1.0, the surface area was reduced to 361.7 m<sup>2</sup>/g and 276.3 m<sup>2</sup>/g, respectively. The dual template P123 and gelatin combination leads to a larger mesoporous structure by expanding the pore diameter. However, a high concentration of gelatin reduced the surface area of silica, presumably due to the saturation of the silica surface with the amine groups, reducing the optimum pore direction. Fig 3(b) showed narrow pore size distribution with a 5–10 nm diameter range for all the mesoporous silica. Increasing the ratio of P123: Gelatin from 1:0 to 1:1 enlarged the pore diameter and formed several pore sizes. The high density of N–H amine group with silanol interactions resulting in different pore shapes (Coradin et al., 2004).

FTIR analysis was carried out on the resulting powder before calcination (Fig 4a) and after calcination at 550 °C (Fig 4b). The uncalcined

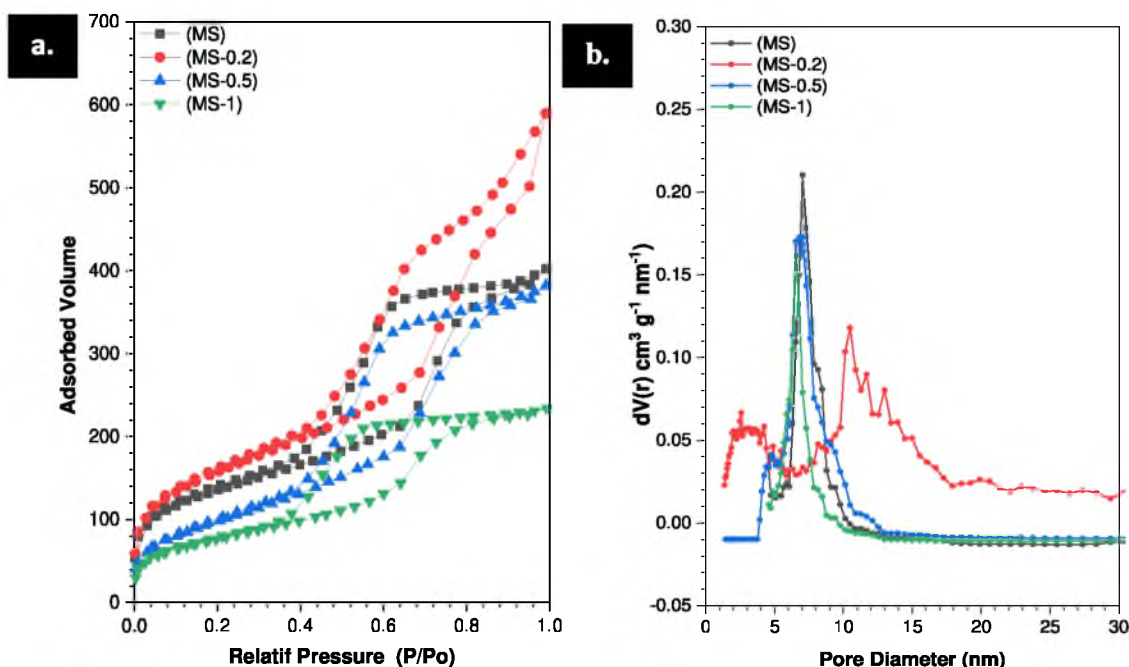


Fig. 3.  $N_2$  adsorption-desorption analysis of the sample mesoporous silica.

Table 1

Textural properties of mesoporous silica.

Samples	S-BET ( $m^2 g^{-1}$ )	S-Meso ( $m^2 g^{-1}$ )	Vp ( $cm^3 g^{-1}$ )	Dp (nm)
MS	482.3	441.1	0.59	7.03
MS-0.2	561.9	485.9	0.72	10.04
MS-0.5	361.7	307.9	0.57	6.8
MS-1	276.3	239.4	0.36	6.5

S-BET, BET-specific surface area; Vp, specific pore volume; Dp, pore diameter, obtained from DFT model.

material showed absorption peaks at  $3466\text{ cm}^{-1}$  ascribed to the N—H bond from gelatin and the O—H bond from P123. The absorption bands at  $962$ ,  $1082$ ,  $798$ , and  $434\text{ cm}^{-1}$  are assigned to Si—OH stretching, non-symmetric and symmetric stretching vibrations of Si—O—Si, and O—Si—O bond, respectively. The specific absorptions demonstrated the presence of block copolymer and gelatin molecules at  $2391$ ,  $2870$ ,  $1674$  and  $1543\text{ cm}^{-1}$  for  $CH_2$ -symmetric and asymmetric absorption, C = O, and N—H bending (Shawky et al., 2016; Han et al., 2018; Trisunaryanti et al., 2016). FTIR spectra of the mesoporous silica after calcination showed the broad absorption band at  $3438\text{ cm}^{-1}$  corresponded to the physisorbed water and the hydroxyl groups, which were accompanied by the OH bending mode at  $1633\text{ cm}^{-1}$ . The bands at  $1103\text{ cm}^{-1}$ ,  $962\text{ cm}^{-1}$ , and  $458\text{ cm}^{-1}$  are assigned to the asymmetric, symmetric stretching, and bending vibrations of Si—O—Si, respectively. All the peaks originating from P123 and gelatin disappeared after calcination, while the Si—O—Si and Si—OH vibration bands gained intensity (Han et al., 2018). The summary of FTIR absorption bands was tabulated in Table 2.

SEM analysis was carried out to analyze the morphology of mesoporous silica after calcination (Fig. 5). Mesoporous silica synthesized from P123 (MS) showed uniform worm-like crystal structures, with the size of MS particles analyzed at  $\sim 10\text{ }\mu\text{m}$ . Introducing the gelatin at 0.2% concentration produced a mixture of cubic and worm-like crystallites. At 0.5% gelatin, the worm-like structures disappeared, producing non-uniform cubic-like morphologies. At 1.0% gelatin, the cube-like structures were more apparent, suggesting the effect of gelatin concentration to transform the morphology of mesoporous silica. A large amount of gelatin increased the size of micelles during the sol-gel synthesis (Kumar et al., 2017; Postnova et al., 2017). Gelatin bound to P123 copolymer

micelles results in a larger silicate ring deposited on the outer surface of micelles, consequently increasing the particle size and transforming the morphology. The histogram of crystallite size distribution showed that the sizes of mesoporous silica were enhanced when using a higher gelatin concentration.

EDX measurement quantitatively analyzed oxygen, silicon, and carbon in mesoporous silica before calcination. Elemental analysis in Fig. 6 indicates the presence of Si at 36.25%, O at 50.26%, and C at 13.49%. The high concentration of carbon on the sample was originated from the carbon in the template.

TEM analysis of mesoporous silica in Fig. 7 showed the formation of hexagonal porosity, which is the characteristic of parallel mesoporous  $p6mm$  space group. The hexagonal structures consisted of long cylindrical pores aligned in the same direction (Wu et al., 2015; Liu and Wang, 2015). The hexagonal pore structure was readily formed in the MS synthesized using P123. The presence of gelatin preserved the hexagonal structure, but the pore diameter appeared larger than the MS without gelatin. The distance between the two adjacent centers of the hexagonal pores was estimated at 5.22 nm for MS synthesized using P123 only (Fig 7a). In the presence of gelatin at 0.2% concentration, the distance between the pores was determined at 7.65 nm (Fig 7b). Further increasing the gelatin concentration to 0.5% and 1% slightly reduced the hexagonal pores to 6.94 nm and 6.62 nm, respectively (Fig 4c, 4d). Nevertheless, the pore sizes of MS from P123: gelatin mixtures were significantly larger than the MS from P123 only.

Thermogravimetric analysis determines the decomposition of P123 and gelatin templates during calcination. The TGA profile of the mesoporous silica material in Fig. 8 showed a two-stage decomposition for each sample. The first decomposition occurred at  $50\text{--}200\text{ }^\circ\text{C}$ , at approximately 3.44% weight loss from water desorption (Kiwilsza et al., 2013). The second decomposition occurred at  $250\text{--}600\text{ }^\circ\text{C}$  with different weight loss percentages. MS reduced 27.79% of its total weight, while MS synthesized using gelatin exhibited 33.28–36.7% weight losses. The mass decrease corresponds to the template decomposition in the mesoporous silica matrix (Mohan et al., 2020; Jin et al., 2014). The DTG results in Fig. 9 indicated a single peak at  $199\text{--}220\text{ }^\circ\text{C}$  for all mesoporous silica samples but at different intensities and temperatures, reflecting the decomposition of template P123 and gelatin (Stawicka et al., 2020). The DTG of the MS-1 sample occurred at a relatively high temperature

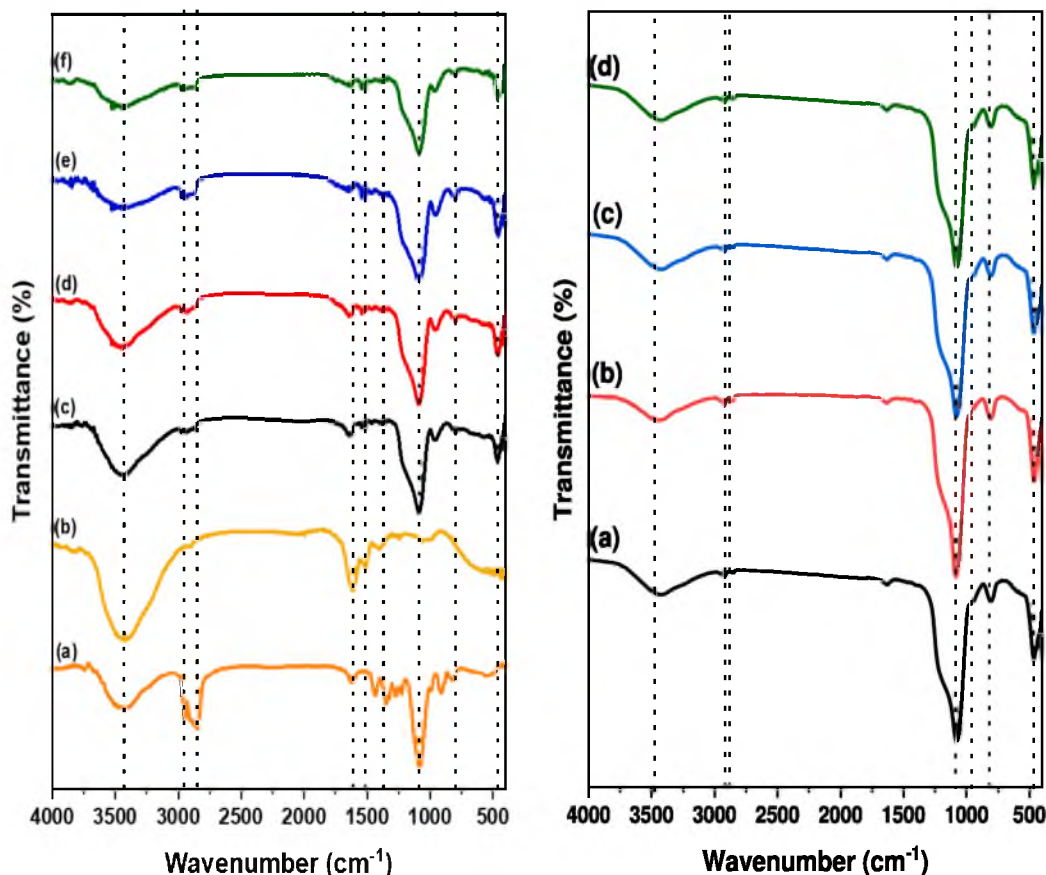


Fig. 4. FTIR spectra of the sample mesoporous silica left before calcination a. P123; b. Gelatin, c. MS; d. MS-0.2; e. MS-0.5; e. MS-1 and right after calcination a. MS; b. MS-0.2; c. MS-0.5, d. MS-1.

Table 2

The characteristic peaks of FTIR of mesoporous silica.

Wavenumber (cm <sup>-1</sup> )	Functional Group (Shawky et al., 2016; Han et al., 2018);
<b>Before calcination</b>	
3466	Hydrogen bonding of NH gelatin and OH from P123
2931	C-H stretching vibration of alkyl chain (P123)
2870	
1674	Vibration Stretching C = O
1523	Vibration N—H
1374	Symmetric Stretching Vibration C—H
1082	Asymmetric Vibration of Si—O—Si
945	Stretching Vibration Si—OH
798	Symmetric Vibration Si—O—Si
434	Bending Vibration Si—O—Si
<b>After Calcination</b>	
3438	Stretching Vibration O—H
1650	Bending Vibration H—O—H
1103	Asymmetric Vibration Si—O—Si
783	Symmetric Vibration S—O—Si
961	Stretching Vibration Si—OH
458	Bending Vibration Si—O—Si

and peak intensity, which may be due to the large particle size that affected the release of energy during the decomposition process.

### 3.2. The interaction of dual template P123 and gelatin for the formation of mesoporous silica

Fig. 10 illustrates the formation of mesoporous silica using P123 and gelatin templates. P123 dissolution in an acidic solution produced a self-

assembly spherical micelle with gelatin due to the formation of hydrogen bonds between the hydroxyl group in P123 and the amine group in gelatin (Ulfa et al., 2020). The hydrogen bonds between P123 and gelatin enlarged the size of micelles compared to the P123 template. The size of gelatin and P123 micelles were responsible for directing silica crystal structure due to the interaction between gelatin and the silica speciation. At low gelatin concentrations, the small size silica particles were formed because of the limited number of available amine groups to interact with silicate. When the amount of gelatin is increased, the availability of the amine group is large enough to interact with SiO<sub>4</sub>, thus forming larger silica-gelatin composites (Coradin et al., 2004; Bele et al., 2002). Gelatin has a natural ability to swell in water, thus prompting further enlargement of micelles. Water adsorption within the micelles enhanced the number of silica bound to the amine group in gelatin. The silicate-gelatin interaction between the nitrogen atoms in the amine group of gelatin and the silicate ions under acidic conditions induces gel network formation for the growth of silica particles (Coradin et al., 2004; Sachithanadam and Joshi, 2014; Bele et al., 2002). This results in the condensation of silicate species which causes the growth of silica particles in the outer micelles. After the calcination, the template decomposition formed mesopores, as evidenced by the N<sub>2</sub> adsorption-desorption analysis. Gelatin also enhanced the mesoporous silica particle sizes from 0.23 μm in MS, to 0.87 μm in MS-1.

### 3.3. Adsorption of methylene blue

#### 3.3.1. Effect of variation dye

The adsorption capacity of mesoporous silica was investigated on different dyes (Fig. 11). The dyes were chosen based on their physical

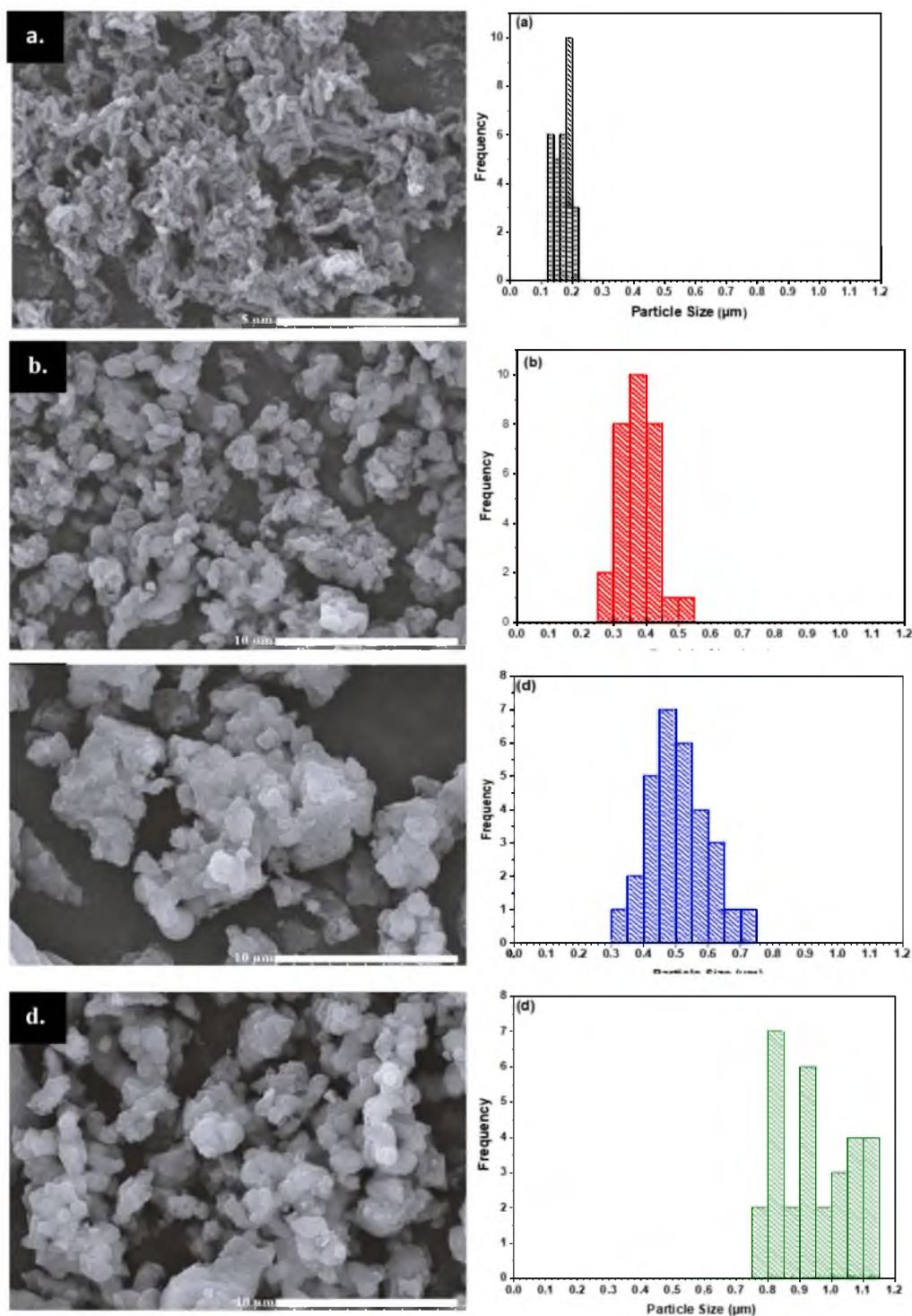


Fig. 5. SEM of mesoporous silica a. MS; b. MS-0.2; c. MS-0.5, d. MS-1.

properties and large molecular structure that requires adsorbent with large pores. Methyl orange (MO) and Congo red (CR) are anionic dyes with molecular weights of 327 g/mol and 696 g/mol, respectively. Meanwhile, methylene blue (MB) and malachite green (MG) are cationic dyes with molecular weights of 319.85 g/mol and 364.911 g/mol, respectively. After 60 min of adsorption, 69 mg/g of methylene blue was adsorbed on mesoporous silica. The value is higher than malachite green at 39.7 mg/g, methyl orange at 4.6 mg/g, and Congo red at 21.46 mg/g. Despite the variation of adsorption capacity when using different types of dyes, the results exhibited the potential of mesoporous silica for

removing organic dyes from aqueous solutions due to its large specific surface area and hierarchical pore structure (Zhou et al., 2015). The methylene blue represented the highest adsorption capacity, indicating mesoporous silica affinity to cationic dyes. The differences may be due to the electrostatic attraction between dye and mesoporous silica and the steric structure of the dyes, which are generally the two key factors affecting the adsorbent efficiency (Iftekhhar et al., 2018). MB and MG are cationic dyes, resulting in more possibilities of being adsorbed on the surface of negatively charged adsorbents through electrostatic interactions. The result of the zeta potential measurement in Fig. 12

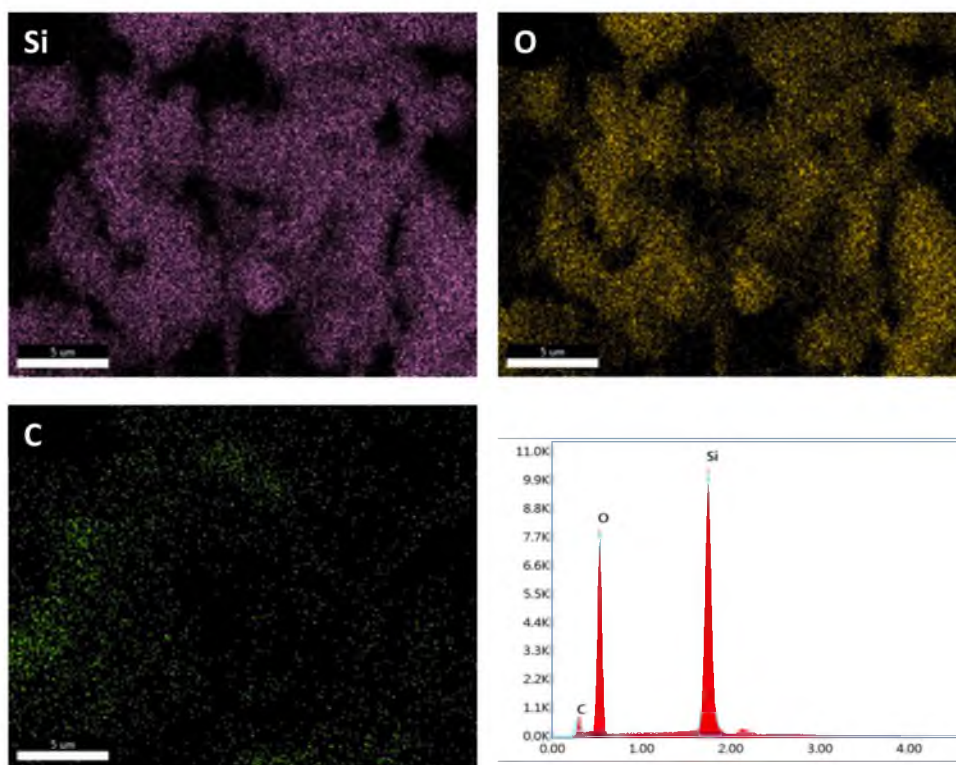


Fig. 6. EDX analysis of the sample MS.

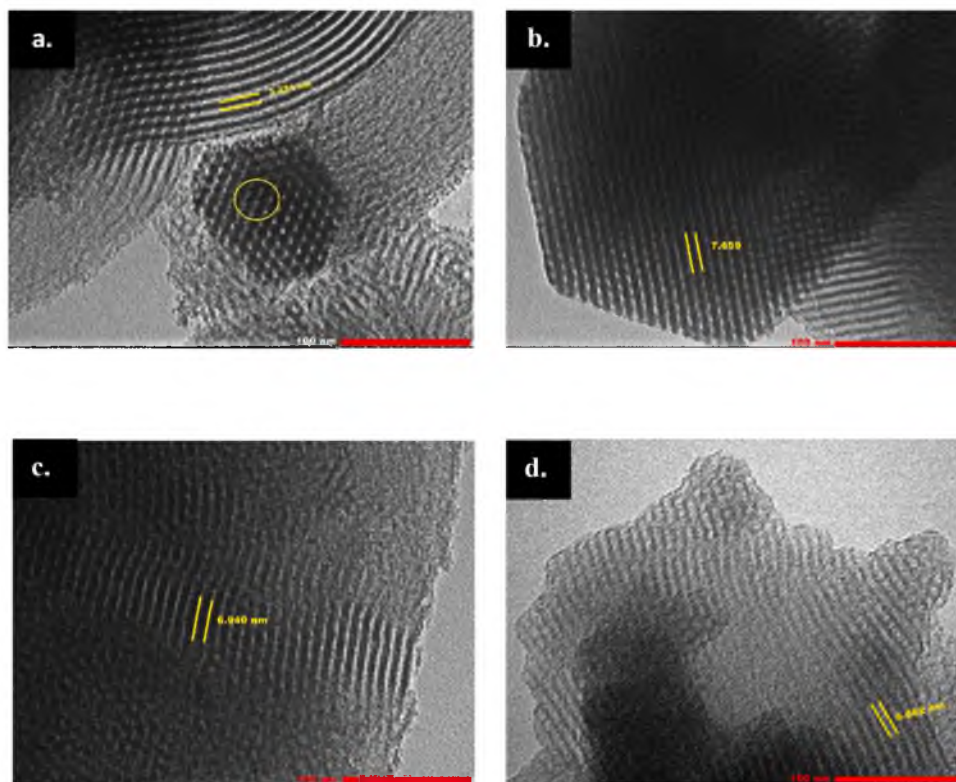


Fig. 7. TEM analysis of the sample mesoporous silica a. MS; b. MS-0.2; c. MS-0.5; and d. MS-1.

indicates that MS has a surface potential of  $-19.6$  mV, as previously reported in silica (Huang et al., 2021). The equilibrium amount of adsorbed methylene blue at 1 hour on mesoporous silica was much

larger than the silica adsorbent reported by Sulistiyo et al. (2017) at 23 mg/g.

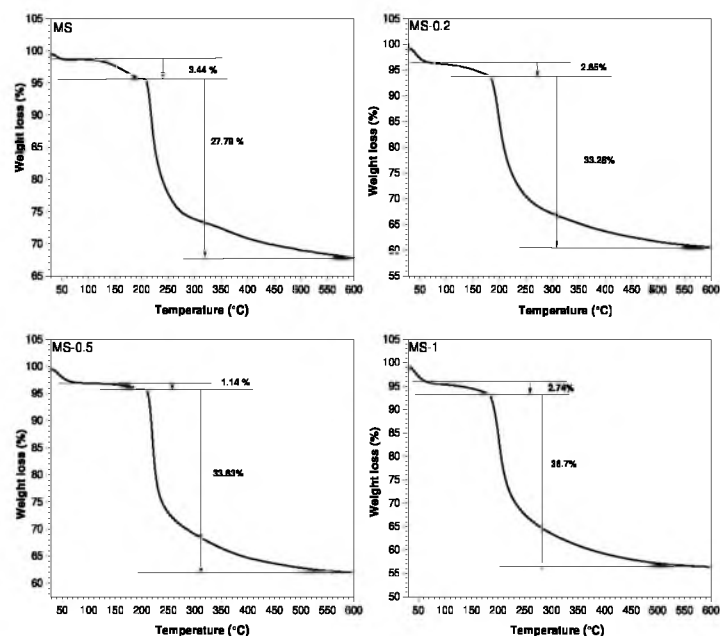


Fig. 8. TGA analysis of the sample mesoporous silica.

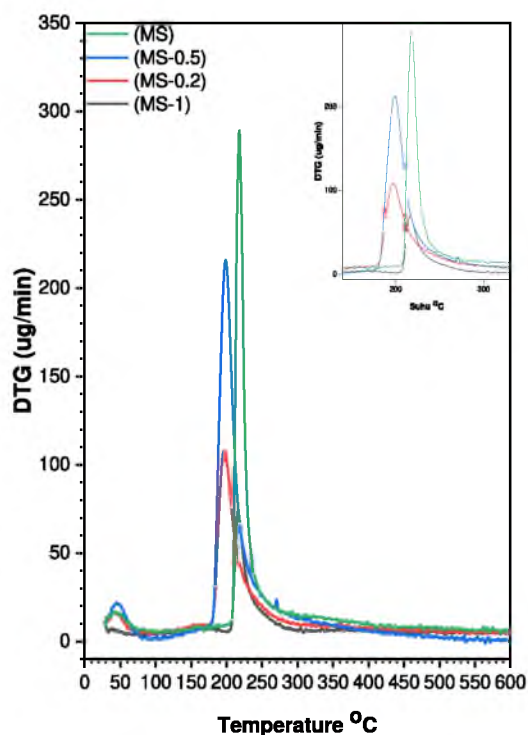


Fig. 9. DTG analysis of the sample mesoporous silica.

### 3.3.2. Effect of adsorbent dosage

Adsorbent dosage is one of the main factors affecting the adsorption efficiency. A high amount of adsorbent increases the available surface area for adsorption. However, it can also be a hindrance due to the adsorption-desorption equilibrium. In this study, the adsorbent dosages were varied at 2.5 mg, 5 mg, 7.5 mg, and 10 mg to determine the optimum amount of adsorbent for methylene blue adsorption in 60 min. The percentage of removal for mesoporous silica obtained at different P123:gelatin ratios and various adsorbent amounts were presented in Fig. 13. The methylene blue removal reached maximum adsorption

when 5 mg and 7.5 mg of adsorbents were used for all the silica. The maximum removal was obtained when using MS-0.2 at 91% with 82.74 mg adsorption capacity, followed by the MS sample at 81.86%, MS-0.5 at 77.71%, and MS-1 at 66.36% removal. The removal efficiency depended on the surface area and porosity of silica. However, a small dose of adsorbent is not sufficient to obtain the optimum removal of methylene blue (Usgodaarachchi et al., 2021)

### 3.3.3. Effect of contact time

Variations of contact time at 2.5, 5, 10, 20, 30, 40, 50 and 60 min were carried out to determine the optimum time for adsorption. The initial concentration of MB solution was 30 mg/L, while using 5 mg adsorbent in 15 mL of solution. Fig. 14 shows the plot between time (minutes) and adsorption capacity (mg/g) for mesoporous silica produced at different P123 to gelatin ratios. The adsorption was rapidly increased from 5 to 30 min before reaching equilibrium at 30 min to give 69 mg/g on MS-0.2 samples. Unoccupied active sites for methylene blue adsorption accelerated the adsorption within the first 30 min. The adsorption slowly decreased up to 60 min. If the adsorbent has reached a state of equilibrium at the optimum contact time, then the prolonged contact time does not contribute to the absorption of dyes (Bernard et al., 2013). However, this can result in more dyes being exchanged after reaching equilibrium, reducing adsorption.

### 3.3.4. Effect of concentration

The concentration of MB solution was varied to obtain the efficiency of mesoporous silica as an adsorbent for the removal of MB in different levels of MB concentrations. MB solution at 10, 30, 50, 70, 90, 120 and 150 mg/L were used, while using 5 mg of MS; MS-0.2; MS-0.5; and MS-1 in 15 mL solution. The optimum contact time for the adsorption was 30 min. Fig. 15 showed that the adsorption capacity of mesoporous silica reached a steady state at a concentration of more than 150 ppm. No adsorption process can occur at high concentrations, where the adsorbate occupies almost all the adsorption sites. Previous research showed that the adsorption capacity of methylene blue using mesoporous silica increased at 25–200 ppm (Zhou et al., 2015). The highest adsorption capacity was shown in the MS-0.2 sample at 150 ppm concentration with a value of 238 mg/g Table 3.

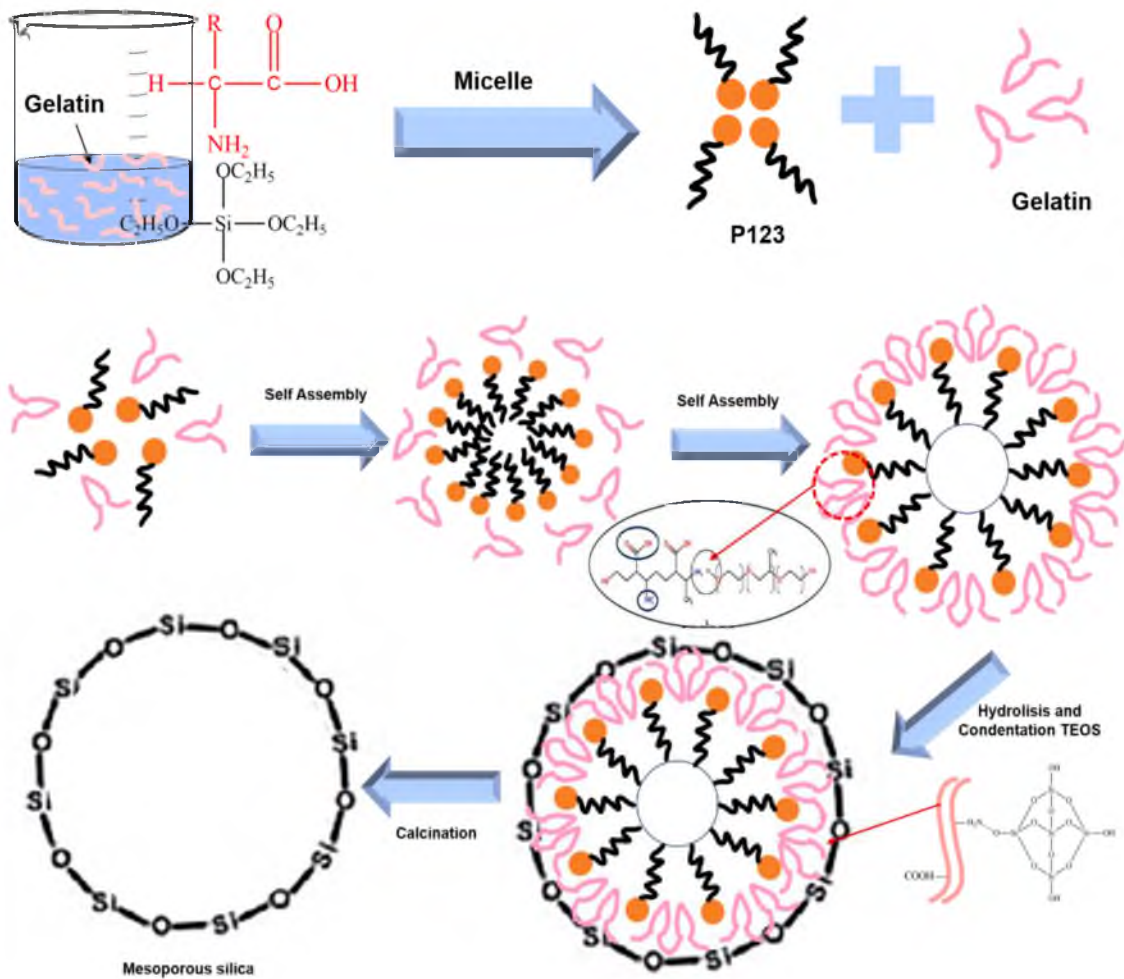


Fig. 10. Formation scheme of mesoporous silica using dual template.

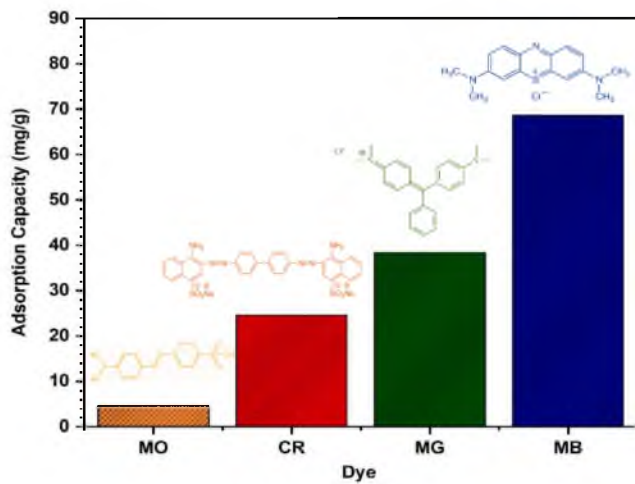


Fig. 11. Adsorption capacity of various dye on MS.

### 3.3.5. Adsorption kinetics

The study of adsorption kinetics is essential to understand the mechanism of adsorption and the rate determining steps such as diffusion control and chemical reaction. The adsorption of dye molecules is a reversible process involving equilibrium between liquid and solid phases. The pseudo first-order and the pseudo second-order kinetic models

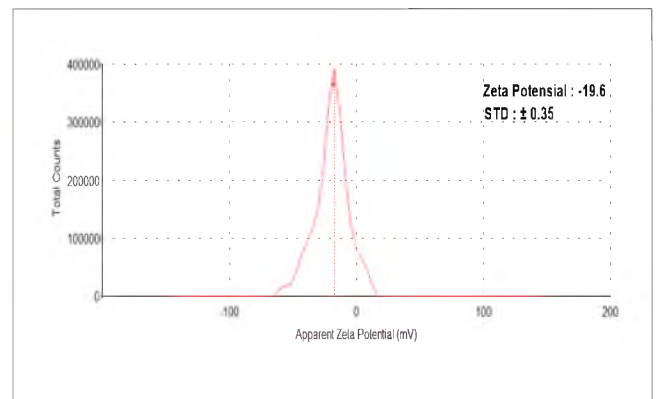


Fig. 12. Zeta Potential Distribution on MS.

Zhai and Li, (2019) are used to simulate the adsorption kinetic behavior of MB on mesoporous silica. The nonlinear pseudo-first-order kinetic and pseudo-second-order kinetic models are expressed as the following Eqs. (5)-(8):

$$qt = qe(1 - e^{-k_1t}) \tag{5}$$

$$qt = \frac{qe^2k_2t}{(1 + qek_2t)} \tag{6}$$

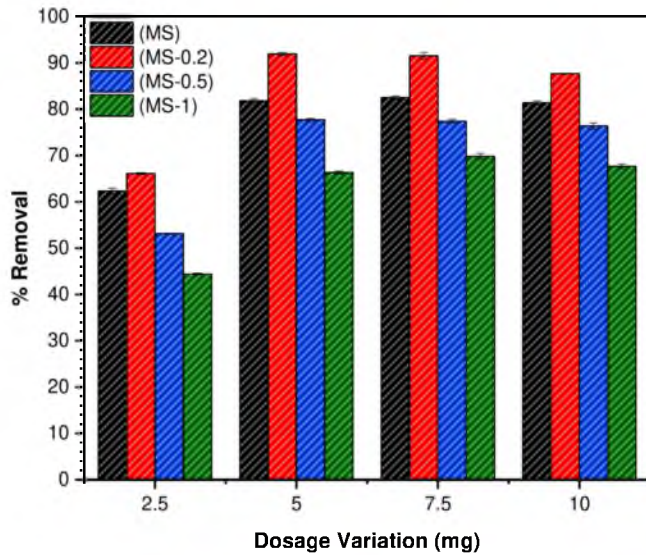


Fig. 13. Adsorption capacity of the sample MS, MS-0.2, MS-0.5, and MS-1 with various dosage.

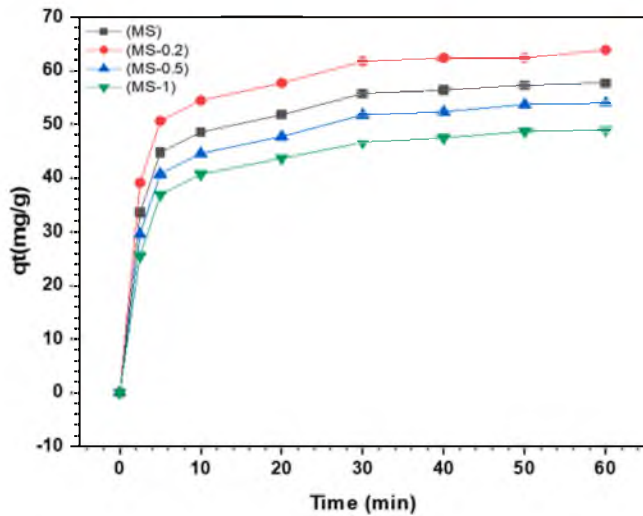


Fig. 14. Adsorption capacity of the sample mesoporous silica variation contact time.

$$\ln(qe - qt) = \ln qe - k_1 t \quad (7)$$

$$\frac{1}{qt} = \frac{1}{k_2 qe^2} + \frac{1}{qe} \quad (8)$$

where  $qe$  and  $qt$  are the amount of methylene blue adsorbed at the equilibrium (mg/g) and at the given adsorption time  $t$ (min), respectively.  $k_1$  defines as the rate constant of pseudo first-order model (1/min) and  $k_2$  is the rate constant of the pseudo second-order model (g/mg min). The nonlinear fitted curves of the two models were shown in Fig. 16, and the values of parameters obtained from the nonlinear curve-fitting results are listed in Table 4. The results exhibited that the adsorption kinetics of all mesoporous silica represented by the pseudo-second-order model, which is based on the correlation coefficients ( $R^2$ ) of the pseudo-second-order model is closer to one than the pseudo-first order model. The pseudo-second-order model showed that the calculated theoretical values of  $qe$  were 58.75 mg/g for MS sample, and 58.75 mg/g for MS-0.2. The calculated equilibrium adsorption capacity  $qe$  from the pseudo-second-order model was more accurate and

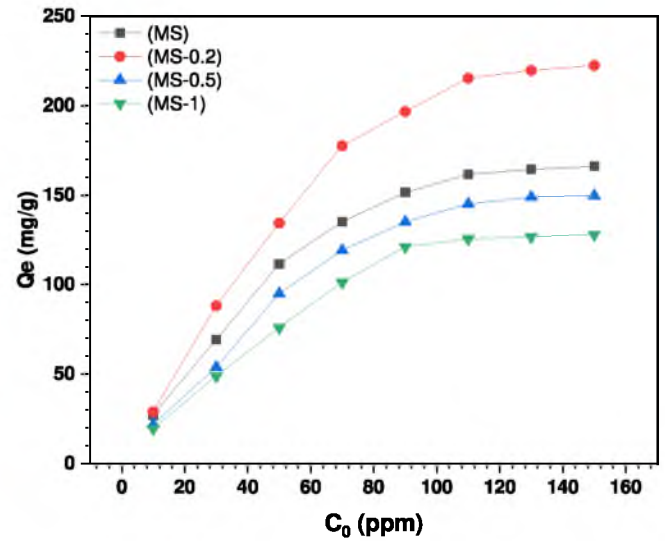


Fig. 15. Adsorption capacity of the sample mesoporous silica variation concentration.

Table 3

The peak temperature and weight of residue of mesoporous silica decomposition at 600 °C.

Sample	$T_{\text{peak}}$ (°C)	$W_{\text{loss1}}$ (water) (%)	$W_{\text{loss2}}$ (fix carbon) (%)	$W_{\text{residue}}$ (ash content) 600 °C (%)
MS	217.17	3.44	27.79	68.77
MS-0.2	196.98	2.85	33.28	63.87
MS-0.5	199.46	1.14	33.83	65.03
MS-1	220.37	2.74	36.7	60.56

consistent with the final experimental  $qt$  value, which further confirmed the validity of this model. The mesoporous silica produced using gelatin has a higher adsorption capacity than the mesoporous silica without gelatin, implying the role of large pore diameter and high surface area in increasing the adsorption capacity Table 5.

### 3.3.6. Isotherm study

The equilibrium adsorption of methylene blue on the mesoporous silica was investigated using the Langmuir and the Freundlich isotherm models, showed in Fig. 17. The Langmuir model assumes monolayer adsorption on the homogeneous surface where the binding sites have equal affinity and energy, and there is no interaction between the adsorbed species Zhai and Li, (2019). The non-linear form of the Langmuir adsorption isotherm model is given as follows Eqs. (9)-(10):

$$qe = \frac{K_L Q_m C_e}{1 + K_L C_e} \quad (9)$$

$$qe = K_F C_e^{\frac{1}{n}} \quad (10)$$

Where  $qe$  and  $Q_m$  represent the equilibrium and the theoretical maximum adsorption capacity (mg/g) of adsorbents, respectively.  $C_e$  is the concentration of ions in solution at equilibrium (mg/L),  $K_L$  defines the Langmuir isotherm constant (L/mg) related to adsorption energy, and  $K_F$  are the Freundlich parameter and heterogeneity factors, respectively. Langmuir model is often applied to the monolayer adsorption with homogeneous and finite modes on the adsorbent, while the Freundlich model is often applied for nonideal sorption on heterogeneous surfaces. It can be observed that the Langmuir model was more suitable for the experimental data since the correlation coefficients of the Langmuir model were closer to 1. However, the Freundlich model has much lower correlation coefficient values. The Langmuir isotherm fitting suggested that the active chelating sites were equal and

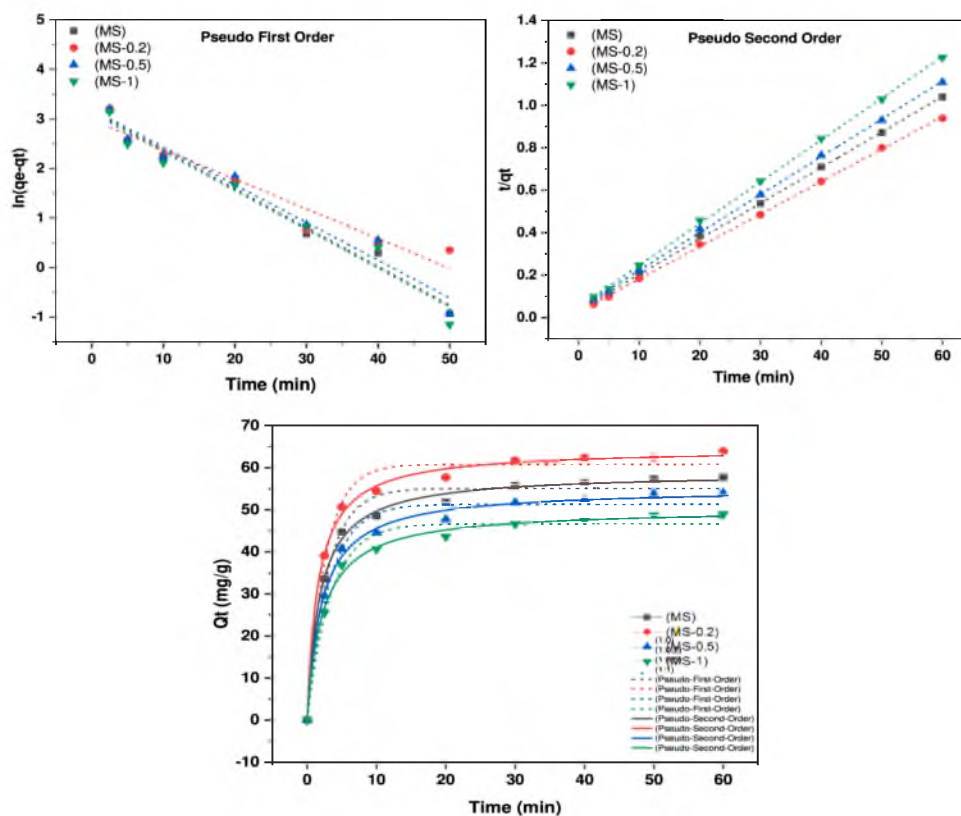


Fig. 16. The adsorption rates of Methylene blue and the corresponding linear-nonlinear form of the pseudo-first-order and pseudo second-order kinetic curves.

Table 4

Kinetic Equation Constant non-linear adsorption on mesoporous silica.

Adsorbents	Pseudo First Order			Pseudo Second Order		
	$k_1$ ( $\text{min}^{-1}$ )	$q_e$ (mg/ g)	$R^2$	$k_2$ (g/ mg.min)	$q_e$ (mg/ g)	$R^2$
MS	0.0784	55.0351	0.97415	0.0093	58.7543	0.9965
MS-0.2	0.0598	60.7521	0.92176	0.0098	64.4583	0.9969
MS-0.5	0.0762	51.266	0.95826	0.0087	55.064	0.9949
MS-1	0.9811	46.626	0.95507	0.0089	50.205	0.9951

Table 5

Non-Linear isotherm parameters of Langmuir and Freundlich.

Adsorbents	Langmuir Model			Freundlich model		
	$kl$ (L/ mg)	$Q_m$ (mg/ g)	$R^2$	$1/n$	$K_f$ (mg/ g)	$R^2$
MS	0.015	251.93	0.9807	0.5213	13.363	0.9304
MS-0.2	0.012	363.63	0.9812	0.5683	14.131	0.9397
MS-0.5	0.012	246.73	0.9746	0.5681	9.5753	0.9314
MS-1	0.0119	212.71	0.9689	0.566	8.2862	0.9268

homogeneously distributed on the surface of the mesoporous channels, and the adsorption occurred via a monolayer formation on the surface. The maximum adsorption uptake of MS-0.2,  $Q_m$  was determined at 392.58 mg/g. The  $Q_m$  of mesoporous silica obtained in this study is much higher than the previously reported adsorption capacity on mesoporous silica materials and other adsorbents, as summarized in Table 6. The high adsorption capacity is due to the formation of a large mesopore diameter for efficient diffusion and a large surface area to provide adsorption sites for MB.

### 3.3.7. Reusability using thermal and chemical regeneration method

The regeneration potential and the reusability of mesoporous silica

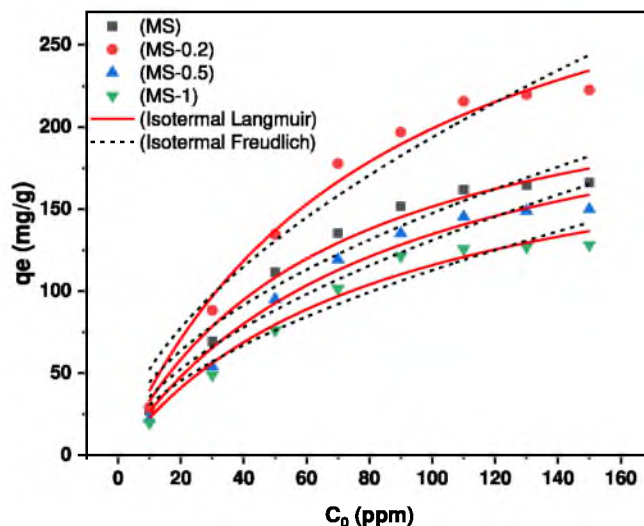


Fig. 17. The adsorption rates of Methylene blue onto mesoporous silica and the corresponding non-linear form of Langmuir and Freundlich curves for adsorption.

were determined using the thermal treatment and chemical desorption with solvent. The MS-0.2 with adsorbed methylene blue was separated from the solution by filtration, dried at 60 °C and calcined at 550 °C for 3 h. Recycling using thermal treatment showed the percentage of MB removal decreases with each reaction cycle (Fig. 18). However, the first and second cycles showed ~90% removal, which indicates the stability of adsorption sites in the mesoporous silica. The desorption of MB from mesoporous silica via the chemical regeneration method was carried out using methanol, HCl, water, and acetone as desorbing agents. The result shows that 74.2% of regeneration efficiency (RE) occurs when using

**Table 6**

Comparison of adsorption capacity of different adsorbents for adsorption methylene blue.

Adsorbent	Adsorption Capacity (mg/g)	Reference
CFA Silica mesopore Nanoparticle	323.62	(Q. Yuan et al., 2019)
Raw KT38 kaolin	52.76	(Mouni et al., 2018)
MGC-4	65.8	(Wang et al., 2014)
Active Carbon	15.59	(Sharma et al., 2009)
Al-SBA15	219.82	(Wu et al., 2015)
Al-MCM-41	277.78	(Zhou et al., 2015)
Graphene oxide-activated carbon	147	(Abd-Elhamid et al., 2019)
Magnetic biochar composite	24.85	(Siddiqui, 2018)
Zeolite-rGO	52.8	(Zhu et al., 2014)
ZFA/HZ	45.09	(Lin et al., 2016)
CaHAp-Alg	77.3	(Guesmi et al., 2018)
Mesoporous silica 1:0	251.93	<b>This research</b>
Mesoporous silica 1:0.2	363.63	<b>This research</b>

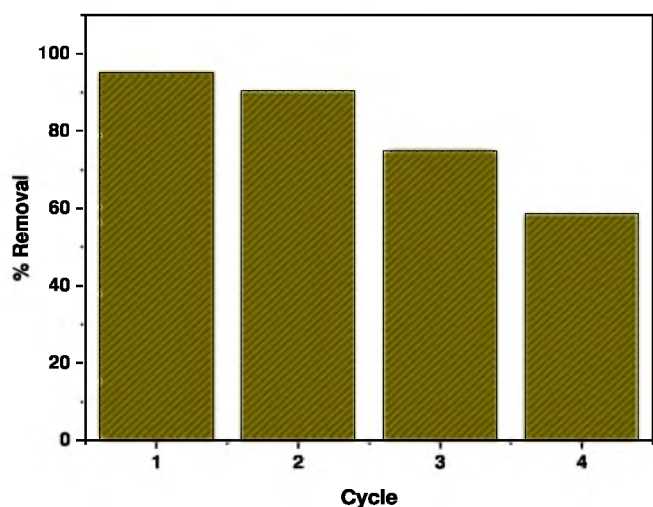


Fig. 18. Reusability study of sample MS-0.2 using a thermal regeneration process.

acetone and 61.4% when using HCl. The amphipathic nature of acetone, which contains hydrophilic (C = O) and hydrophobic groups (-CH<sub>3</sub>), accounts for its good desorbing agent (Xing et al., 2017). Meanwhile, under the acidic condition (HCl), a higher concentration of H<sub>3</sub>O<sup>+</sup> increases positive charges on the surface of the adsorbent. The cationic dye molecules are drawn to negatively charged adsorbent surface particles, and the desorption happens as a result of electrostatic repulsion.

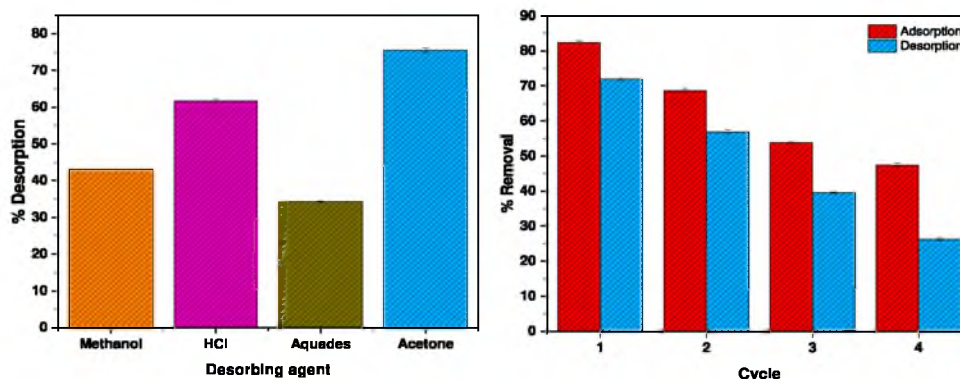


Fig. 19. Desorption study of sample MS-0.2 using variation desorbing agent.

(Momina and Suzylawati, 2020). The adsorption-desorption cycles were repeated four times using acetone to verify the reusability of the mesoporous silica. Fig. 19 shows the adsorption capacities of mesoporous silica for methylene blue over four successive adsorption-desorption cycles. The results indicated that the adsorption capacity of mesoporous silica decreased with prolonged cycles to give 45.1% removal after four cycles. Although the efficiency was reduced, mesoporous silica still showed good potential as a reusable adsorbent for removing methylene blue from wastewater.

### 3.3.8. Adsorption mechanism

FTIR analysis was carried out to investigate the interaction between methylene blue and mesoporous silica shown in Fig. 20. Methylene blue contained O—H, C = C, C = N, C = S, C—S, and C—H functionalities that

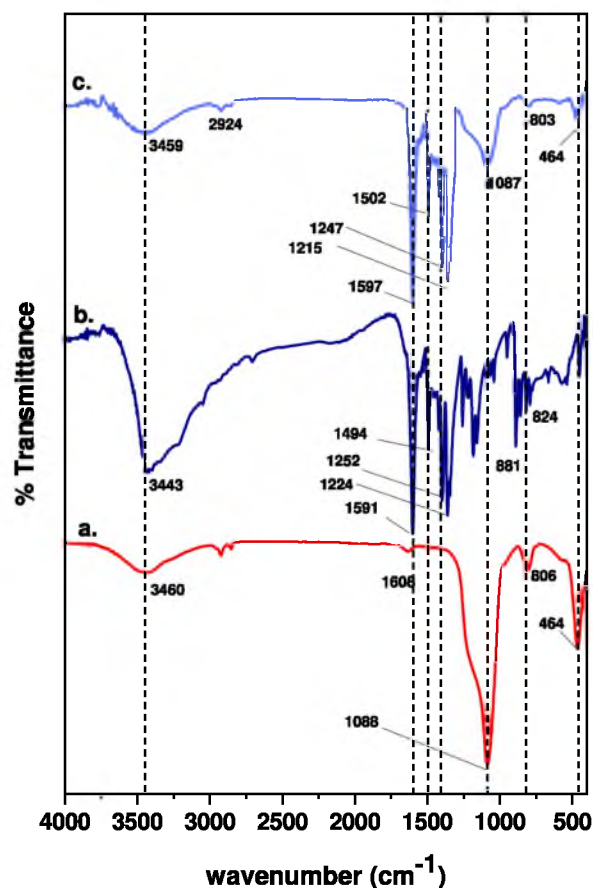
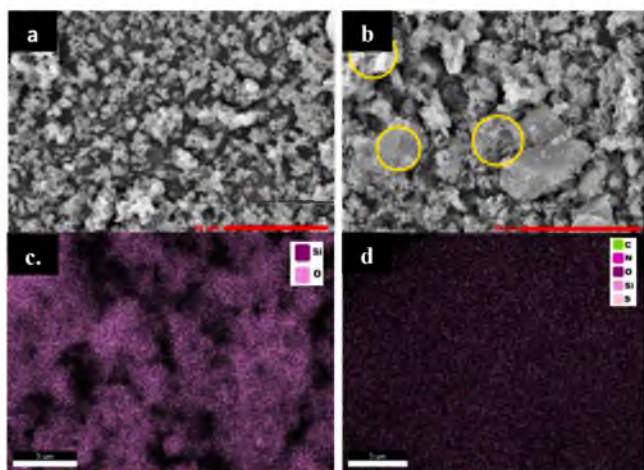


Fig. 20. FTIR Spectra of a. MS-0.2; b. MB; and c. MB-MS-0.2.

**Table 7**  
Functional Group Spectra of MS, MB, and MB-MS-0.2.

Assignments	Wavenumber (cm <sup>-1</sup> )		
	MS-0.2	MB	MB-MS-0.2
Overlapping stretching vibration of -NH/OH	3460	3443	3459
Stretching vibration of C = C side ring	–	1594	1597
Stretching vibration of -CH <sub>2</sub> or CH <sub>3</sub>	–	1494–1500	1502
Stretching vibration of -CN	–	1252	1247
Stretching vibration of -N-N	–	1244	1215
Stretching vibration of -CH	–	1176	–
Stretching vibration of -C-S-C	–	1064	–
Bending vibration of C–H out of plane	–	881 and 824	–
Bending Vibration H–O–H	1608	–	–
Asymmetric Vibration Si–O–Si	1088	–	1087
Symmetric Vibration Si–O–Si	806	–	803
Bending Vibration Si–O–Si	464	–	464



**Fig. 21.** SEM-EDX before and after adsorption: MS-0.2 (a,c) and MB-MS-0.2 (b,d).

**Table 8**  
Elemental analysis before and after adsorption.

Element	Weight (%)	
	MS-0.2	MB-MS-0.2
Si	40.89	32.41
O	59.11	52.84
C	–	8.63
N	–	3.9
S	–	2.22

were able to interact with mesoporous silica surfaces during adsorption (Pradhan et al., 2017). FTIR analysis of MB showed the strong adsorption bands at 1594 cm<sup>-1</sup> and 1252 cm<sup>-1</sup> ascribed to the stretching vibration of C = C, and C–N bonds in the heterocyclic of MB, respectively. The functional group of mesoporous silica, MB, and MB adsorbed MS-0.2 were summarized in Table 7. Analysis of mesoporous silica obtained at 1:0.2 ratio after MB adsorption showed the FTIR bands of mesoporous silica appeared at similar wavenumber. The FTIR also showed the appearance of 1543 cm<sup>-1</sup> and 1378 cm<sup>-1</sup> bands ascribed to the stretching vibration of C = N and CH<sub>2</sub> of MB adsorbed on the silica. Two suggested mechanisms were proposed to describe the adsorbent-adsorbate interaction based on the FTIR analysis from the adsorbed methylene blue on mesoporous silica. The adsorption of methylene blue on mesoporous silica occurs via the formation of a hydrogen bridge between the lone pair electrons of nitrogen atoms in methylene blue with the Si–OH in mesoporous silica. In addition,

methylene blue is also adsorbed through the electrostatic attraction between the negative charge O<sup>-</sup> (SiO<sub>2</sub> structure) and the positive charge of N<sup>+</sup> (methylene blue structure) (Lyu et al., 2020; N. Yuan et al., 2019). Due to the absence of S–O bonds from FTIR analysis, there is no donor-acceptor evidence of interactions between electron-deficient sulfur atoms in MB with SiO<sub>2</sub>.

Fig. 21 and Table 8 show the SEM-EDX analysis of MS-0.2 before and after adsorption and the elemental composition. As previously discussed in the SEM characterization section, the mesoporous silica has a worm-like morphology with uniform microcrystallites. Following the adsorption with MB molecules, the mesoporous silica appeared as non-uniform aggregates. EDS analysis indicated the variation in the elemental composition of MS and MS-0.2. MS has 36.25% Si and 50.26% O, while MS-0.2 has 40.89% Si and 59.11% O. A high concentration of oxygen in MS-0.2 provides more possibility of the interaction between oxygen atoms in silica with the hydrogen atoms in MB, to increase the adsorption capacity. High composition of N and S atoms at 3.9% and 2.22% were observed on MS-0.2, indicating the presence of methylene blue on the silica.

#### 4. Conclusion

The synthesis of mesoporous silica using dual template P123:gelatin has been successfully carried out, indicating the ability of gelatin to form large mesopores in silica for efficient dye removal. The optimum ratio between P123 and gelatin is varied to determine the best combination for enlarging the mesopore size while maintaining a high surface area. Amine functional groups in gelatin produced electrostatic interaction with the silicate ions precursor for constructing mesoporosity. The morphology of mesoporous silica changes from worm-like to cubic-like structure with increasing gelatin concentration. The particle size enlarged from 0.23 μm to 0.87 μm, while the surface area improved from 200 to 560 m<sup>2</sup>/g surface area with optimization of P123:gelatin ratios. Gelatin enlarged the diameter of the mesopore channel to reach ~10 nm, improving the diffusion of MB molecules. The largest adsorption capacity was obtained on mesoporous silica synthesized at a 1:0.2 ratio with the *Q<sub>m</sub>* value of 363.63 mg/g. The adsorption kinetics followed the pseudo second order with the Langmuir model. The use of gelatin as a green template improved the physicochemical properties of mesoporous silica, opening up new opportunities for naturally occurring surfactants in material synthesis.

#### Declaration of Competing Interest

The authors declare that they have no known competing financial interests or personal relationships that could have appeared to influence the work reported in this article.

#### Acknowledgments

The author would like to thank the scheme Program Penelitian Kolaborasi Indonesia (PPKI) Institut Teknologi Sepuluh Nopember (ITS) under project No. 102.1/UN27.22/HK.07.00/2021 for Didik Praseptyoko, in collaboration with Universitas Sebelas Maret (UNS) and Universitas Gadjah Mada (UGM).

#### References

- Abd-Elhamid, A.I., Kamoun, E.A., El-Shanshory, A.A., Soliman, H.M.A., Aly, H.F., 2019. Evaluation of graphene oxide-activated carbon as effective composite adsorbent toward the removal of cationic dyes: composite preparation, characterization and adsorption parameters. *J. Mol. Liq.* 279, 530–539. <https://doi.org/10.1016/J.MOLLIQ.2019.01.162>.
- Albayati, T.M., Salih, I.K., Alazzawi, H.F., 2019. Synthesis and characterization of a modified surface of SBA-15 mesoporous silica for a chloramphenicol drug delivery system. *Heliyon* 5, e02539. <https://doi.org/10.1016/J.HELIYON.2019.E02539>.
- Barranco-García, R., Ferreira, A.E., Ribeiro, M.R., Lorenzo, V., García-Peñas, A., Gómez-Elvira, J.M., Pérez, E., Cerrada, M.L., 2018. Hybrid materials obtained by in situ

- polymerization based on polypropylene and mesoporous SBA-15 silica particles: catalytic aspects, crystalline details and mechanical behavior. *Polymer (Guildf)* 151, 218–230. <https://doi.org/10.1016/J.POLYMER.2018.07.072>.
- Bele, M., Gaberscek, M., Dominko, R., Drogenik, J., Zupan, K.Y., Komac, P., Kocevar, K., Musevic, I., Pejovnik, S., 2002. Gelatin-pretreated carbon particles for potential use in lithium ion batteries. *Carbon* 40, 1117–1122. [https://doi.org/10.1016/S0008-6223\(01\)00257-3](https://doi.org/10.1016/S0008-6223(01)00257-3).
- Bernard, E., Jimoh, A., Odigure, J., Obofoni, 2013. Heavy metals removal from industrial wastewater by activated carbon prepared from coconut shell. *Res. J. Chem. Sci.* 3, 3–9. <https://www.researchgate.net/publication/289401355> (accessed July 12, 2022).
- Chen, C.H., Shimom, D., Lee, J.J., Didas, S.A., Mehta, A.K., Sievers, C., Jones, C.W., Hayes, S.E., 2017. Spectroscopic characterization of adsorbed 13CO<sub>2</sub> on 3-aminopropylsilyl-modified SBA15 mesoporous silica. *Environ. Sci. Technol.* 51, 6553–6559. [https://doi.org/10.1021/ACS.EST.6B06605/SUPPL\\_FILE/ES6B06605\\_S1\\_001.PDF](https://doi.org/10.1021/ACS.EST.6B06605/SUPPL_FILE/ES6B06605_S1_001.PDF).
- Coradin, T., Bah, S., Livage, J., 2004. Gelatine/silicate interactions: from nanoparticles to composite gels. *Colloids Surf. B. Biointerfaces.* 35, 53–58. <https://doi.org/10.1016/J.COLSURFB.2004.02.008>.
- Dubey, R.S., Rajesh, Y.B.R.D., More, M.A., 2015. Synthesis and characterization of SiO<sub>2</sub> nanoparticles via sol-gel method for industrial applications. *Mater. Today Proc.* 2, 3575–3579. <https://doi.org/10.1016/J.MATPR.2015.07.098>.
- Etchepare, R., Zaneti, R., Azevedo, A., Rubio, J., 2015. Application of flocculation–flotation followed by ozonation in vehicle wash wastewater treatment/disinfection and water reclamation. *Desalin. Water Treat.* 56, 1728–1736. <https://doi.org/10.1080/19443994.2014.951971>.
- Guesmi, Y., Agougui, H., Lafi, R., Jabli, M., Hafiane, A., 2018. Synthesis of hydroxyapatite-sodium alginate via a co-precipitation technique for efficient adsorption of Methylene Blue dye. *J. Mol. Liq.* 249, 912–920. <https://doi.org/10.1016/J.MOLLIQ.2017.11.113>.
- Han, P., Liu, T., Ji, X., Tang, S., 2018. Morphology-controlled synthesis of mesoporous silica with co-template of surfactant P123 and ionic liquid [Dmim]Cl. *Chinese Chem. Lett.* 29, 1305–1309. <https://doi.org/10.1016/j.ccl.2017.10.042>.
- Han, X., Wang, Y., Zhang, N., Meng, J., Li, Y., Liang, J., 2021. Facile synthesis of mesoporous silica derived from iron ore tailings for efficient adsorption of methylene blue. *Colloids Surfaces A Physicochem. Eng. Asp.* 617. <https://doi.org/10.1016/j.colsurfa.2021.126391>.
- He, Z., Alexandridis, P., 2018. Micellization thermodynamics of Pluronic P123 (EO<sub>20</sub>PO<sub>70</sub>EO<sub>20</sub>) amphiphilic block copolymer in aqueous Ethylammonium nitrate (EAN) solutions. *Polymers (Basel)* 10. <https://doi.org/10.3390/polym10010032>.
- Huang, J., Lai, W., Wang, Q., Tang, Q., Hu, C., Zhou, M., Wang, F., Xie, D., Zhang, Q., Liu, W., Zhang, Z., Zhang, R., 2021. Effective triple-negative breast cancer targeted treatment using iRGD-modified RBC membrane-camouflaged nanoparticles. *Int. J. Nanomedicine.* 16, 7497–7515. <https://doi.org/10.2147/IJN.S321071>.
- Ifekhar, S., Ramasamy, D.L., Srivastava, V., Asif, M.B., Sillanpää, M., 2018. Understanding the factors affecting the adsorption of Lanthanum using different adsorbents: a critical review. *Chemosphere* 204, 413–430. <https://doi.org/10.1016/J.CHEMOSPHERE.2018.04.053>.
- Jin, J.S., Cao, L., Su, G.X., Xu, C.Y., Zhang, Z.T., Gao, X.H., Liu, H.H., Liu, H.T., 2014. A facile strategy to recycle template P123 from mesoporous aluminosilicates by ultrasonic extraction. *Ultrason. Sonochem.* 21, 1688–1695. <https://doi.org/10.1016/J.ULTSONCH.2014.02.025>.
- Karakilic, P., Toyoda, R., Kaptejin, F., Nijmeijer, A., Winnubst, L., 2019. From amorphous to crystalline: transformation of silica membranes into silicite-1 (MF1) zeolite layers. *Microporous Mesoporous Mater.* 276, 52–61. <https://doi.org/10.1016/J.MICROMESO.2018.09.020>.
- Karthik, R., Muthazhilan, R., Jaffar Hussain, A., Ramalingam, K., Rekha, V., 2015. Effective removal of Methylene Blue dye from water using three different low-cost adsorbents. *New Pub Balaban.* 57, 10626–10631. <https://doi.org/10.1080/19443994.2015.1039598>.
- Kiwilsza, A., Mielcarek, J., Pajzderska, A., Waosicki, J., 2013. Ordered mesoporous silica material SBA-15: loading of new calcium channel blocker-lacidipine. *J. Microencapsul.* 30, 21–27. <https://doi.org/10.3109/02652048.2012.692401>.
- Kumar, S., Malik, M.M., Purohit, R., 2017. Synthesis Methods of Mesoporous Silica Materials. *Mater. Today Proc.* 4, 350–357. <https://doi.org/10.1016/j.matpr.2017.01.032>.
- Li, J., Wu, E., 2009. Adsorption of hydrogen on porous materials of activated carbon and zeolite NaX crossover critical temperature. *J. Supercrit. Fluids.* 49, 196–202. <https://doi.org/10.1016/J.SUPFLU.2008.12.015>.
- Lin, L., Lin, Y., Li, C., Wu, D., Kong, H., 2016. Synthesis of zeolite/hydrous metal oxide composites from coal fly ash as efficient adsorbents for removal of methylene blue from water. *Int. J. Miner. Process. C* 32–40. <https://doi.org/10.1016/J.MINPRO.2016.01.010>.
- Liu, R., Wang, C.A., 2015. Synthesis of hollow mesoporous silica spheres with radially aligned mesochannels and tunable textural properties. *Ceram. Int.* 41, 1101–1106. <https://doi.org/10.1016/j.ceramint.2014.09.035>.
- Lyu, R., Zhang, C., Xia, T., Chen, S., Wang, Z., Luo, X., Wang, L., Wang, Y., Yu, J., Wang, C.W., 2020. Efficient adsorption of methylene blue by mesoporous silica prepared using sol-gel method employing hydroxyethyl cellulose as a template. *Colloids Surfaces A Physicochem. Eng. Asp.* 606, 125425. <https://doi.org/10.1016/J.COLSURFA.2020.125425>.
- Mahony, O., Yue, S., Turdean-Ionescu, C., Hanna, J.V., Smith, M.E., Lee, P.D., Jones, J.R., 2014. Silica gelatin hybrids for tissue regeneration: inter-relationships between the process variables. *J. Sol-Gel Sci. Technol.* 69, 288–298. <https://doi.org/10.1007/S10971-013-3214-3/FIGURES/9>.
- Mohan, A., Rout, L., Thomas, A.M., Peter, J., Nagappan, S., Parambadath, S., Ha, C.S., 2020. Palladium nanoparticles-anchored dual-responsive SBA-15-PNIPAM/PMAA nanoreactor: a novel heterogeneous catalyst for a green Suzuki–Miyaura cross-coupling reaction. *RSC Adv.* 10, 28193–28204. <https://doi.org/10.1039/D0RA05786J>.
- Momina, S., Mohammad, Suzyulawati, I., 2020. Study of the adsorption/desorption of MB dye solution using bentonite adsorbent coating. *J. Water Process Eng.* 34, 101155. <https://doi.org/10.1016/J.JWPE.2020.101155>.
- Mouni, L., Belkhir, L., Bollinger, J.C., Bouzaza, A., Assadi, A., Tirri, A., Dahmoune, F., Madani, K., Remini, H., 2018. Removal of methylene blue from aqueous solutions by adsorption on Kaolin: kinetic and equilibrium studies. *Appl. Clay Sci.* 153, 38–45. <https://doi.org/10.1016/J.CLAY.2017.11.034>.
- Postnova, I., Sarin, S., Silantyev, V., Shechipunov, Y., 2017. Evolution of block copolymer template structure during the synthesis of ordered mesoporous silica. *Colloid Polym. Sci.* 4, 549–554. <https://doi.org/10.1007/S00396-017-4043-7>.
- Pradhan, A.C., Paul, A., Rao, G.R., 2017. Sol-gel-cum-hydrothermal synthesis of mesoporous Co-Fe@Al<sub>2</sub>O<sub>3</sub>-MCM-41 for methylene blue remediation. *J. Chem. Sci.* 129, 381–395. <https://doi.org/10.1007/S12039-017-1230-5>.
- Rafatullah, M., Sulaiman, O., Hashim, R., Ahmad, A., 2010. Adsorption of methylene blue on low-cost adsorbents: a review. *J. Hazard. Mater.* 177, 70–80. <https://doi.org/10.1016/J.JHAZMAT.2009.12.047>.
- Rajendhiran, R., Deivasigamani, V., Palanisamy, J., Masan, S., Pitchaiya, S., 2021. Terminalia catappa and carissa carandas assisted synthesis of TiO<sub>2</sub> nanoparticles – a green synthesis approach. *Mater. Today Proc.* 45, 2232–2238. <https://doi.org/10.1016/J.MATPR.2020.10.223>.
- Rayati, S., Nafarieh, P., Amini, M.M., 2018. The synthesis, characterization and catalytic application of manganese porphyrins bonded to novel modified SBA-15. *New J. Chem.* 42, 6464–6471. <https://doi.org/10.1039/C8NJ00743H>.
- Rehman, F., Volpe, P.L.O., Airoldi, C., 2014. The applicability of ordered mesoporous SBA-15 and its hydrophobic glutaraldehyde-bridge derivative to improve ibuprofen loading in releasing system. *Colloids Surf. B. Biointerfaces.* 119, 82–89. <https://doi.org/10.1016/J.COLSURFB.2014.03.043>.
- Sachithanadam, M., Joshi, S.C., 2014. A new phenomenon of compressive strain recovery in gelatin-silica aerogel composites with sds. *Procedia Eng.* 75, 51–55. <https://doi.org/10.1016/J.PROENG.2013.11.010>.
- Sari Yilmaz, M., 2022. Graphene oxide/hollow mesoporous silica composite for selective adsorption of methylene blue. *Microporous Mesoporous Mater.* 330, 111570. <https://doi.org/10.1016/J.MICROMESO.2021.111570>.
- Sharma, Y.C., Uma, Upadhyay, S.N., 2009. Removal of a cationic dye from wastewaters by adsorption on activated carbon developed from coconut coir. *Energy Fuels* 23, 2983–2988. <https://doi.org/10.1021/EF9001132>.
- Shawky, S.M., Abo-ElHassan, A.A., Lill, H., Bald, D., F.E.L-Khamisy, S., Ebeid, E.-Z.M., 2016. Efficient loading and encapsulation of anti-tuberculosis drugs using multifunctional mesoporous silicate nanoparticles. *J. Nanosci. Curr. Res.* 1, 1–9. <https://doi.org/10.4172/2572-0813.1000103>.
- Siddiqui, S.H., 2018. The removal of Cu<sup>2+</sup>, Ni<sup>2+</sup> and Methylene Blue (MB) from aqueous solution using Luffa Actungula Carbon: kinetics, thermodynamic and isotherm and response methodology. *Groundw. Sustain. Dev.* 6, 141–149. <https://doi.org/10.1016/J.GSD.2017.12.008>.
- Stawicka, K., Gierada, M., Gajewska, J., Tielen, F., Ziolk, M., 2020. The importance of the reactivity of silica on the selectivity of MPTMS on the example of SBA-15. *Appl. Surf. Sci.* 513. <https://doi.org/10.1016/J.APSUSC.2020.145802>.
- Sulistiyono, Y.A., Andriana, N., Piluharto, B., Zulfikar, Z., 2017. Silica gels from coal fly ash as methylene blue adsorbent: isotherm and kinetic studies. *Bull. Chem. React. Eng. & Catal.* 12, 263–272. <https://doi.org/10.9767/brec.12.2.766.263-272>.
- Tako, M., Tamaki, Y., Teruya, T., Takeda, Y., 2014. The principles of starch gelatinization and retrogradation. *Food Nutr. Sci.* 05, 280–291. <https://doi.org/10.4236/FNS.2014.53035>.
- Tebuhjuluw, H., Subagyo, R., Kusumawati, Y., Prasetyoko, D., 2022. The impregnation of ZnO onto ZSM-5 derived from red mud for photocatalytic degradation of methylene blue. *Sustain. Environ. Res.* 32, 1–12. <https://doi.org/10.1186/S42834-021-00113-8/FIGURES/10>.
- Trisunaryanti, W., Lisna, P.S., Kartini, I., Sutarno, I.I., Falah, Triyono, 2016. Extraction of gelatin from bovine bone and its use as template in synthesis of mesoporous silica. *Asian J. Chem.* 28, 996–1000. <https://doi.org/10.14233/AJCHEM.2016.19561>.
- M. Ulfa, D. Prasetyoko, H. Bahruji, R.E. Nugraha, Green synthesis of hexagonal hematite (α-Fe<sub>2</sub>O<sub>3</sub>) flakes using pluronic F127-gelatin template for adsorption and photodegradation of Ibuprofen, (2021). <https://doi.org/10.20944/PREPRINTS202110.0138.V1>.
- Ulfa, M., Prasetyoko, D., Mahadi, A.H., Bahruji, H., 2020. Size tunable mesoporous carbon microspheres using Pluronic F127 and gelatin as co-template for removal of ibuprofen. *Sci. Total Environ.* 711, 135066. <https://doi.org/10.1016/J.SCITOTENV.2019.135066>.
- Ulfa, M., Trisunaryanti, W., Falah, I.I., Kartini, I., 2018. Wormhole-like mesoporous carbons from gelatine as multistep infiltration effect. *Indones. J. Chem.* 16, 239–242. <https://doi.org/10.22146/IJC.21137>.
- Uppandar, G., Dutta, S., Bhattacharya, P., Dutta, A., 2017. Bioremediation of methylene blue dye using *Bacillus subtilis* MTCC 441. *Water Sci. Technol.* 75, 1572–1583. <https://doi.org/10.2166/WST.2017.031>.
- Usgodaarachchi, L., Thambiliyagodage, C., Wijesekera, R., Bakker, M.G., 2021. Synthesis of mesoporous silica nanoparticles derived from rice husk and surface-controlled amine functionalization for efficient adsorption of methylene blue from aqueous solution. *Curr. Res. Green Sustain. Chem.* 4, 100116. <https://doi.org/10.1016/J.CRGSC.2021.100116>.
- Veisi, H., Tamoradi, T., Karmakar, B., Hemmati, S., 2020. Green tea extract-modified silica gel decorated with palladium nanoparticles as a heterogeneous and recyclable

- nanocatalyst for Buchwald-Hartwig C–N cross-coupling reactions. *J. Phys. Chem. Solids*. 138, 109256. <https://doi.org/10.1016/J.JPCS.2019.109256>.
- Wang, P., Cao, M., Wang, C., Ao, Y., Hou, J., Qian, J., 2014. Kinetics and thermodynamics of adsorption of methylene blue by a magnetic graphene-carbon nanotube composite. *Appl. Surf. Sci.* 290, 116–124. <https://doi.org/10.1016/J.APSUSC.2013.11.010>.
- Wu, Z., Lu, Q., Fu, W.H., Wang, S., Liu, C., Xu, N., Wang, D., Wang, Y.M., Chen, Z., 2015. Fabrication of mesoporous Al-SBA-15 as a methylene blue capturer via a spontaneous infiltration route. *New J. Chem.* 39, 985–993. <https://doi.org/10.1039/c4nj01473a>.
- Wüstneck, R., Krägel, J., 1998. Characterisation of gelatin/surfactant interaction and its relevance to liquid film coating. *Stud. Interface Sci.* 7, 433–490. [https://doi.org/10.1016/S1383-7303\(98\)80058-6](https://doi.org/10.1016/S1383-7303(98)80058-6).
- Xie, Y., Kocaefer, D., Chen, C., Kocaefer, Y., 2016. Review of research on template methods in preparation of nanomaterials. *J. Nanomater.* 2016. <https://doi.org/10.1155/2016/2302595>.
- Xing, X., Qu, H., Shao, R., Wang, Q., Xie, H., 2017. Mechanism and kinetics of dye desorption from dye-loaded carbon (XC-72) with alcohol-water system as desorbent. *Water Sci. Technol.* 76, 1243–1250. <https://doi.org/10.2166/wst.2017.268>.
- Xue, H., Wang, X., Xu, Q., Dhaouadi, F., Sellaoui, L., Seliem, M.K., Ben Lamine, A., Belmabrouk, H., Bajahzar, A., Bonilla-Petriciolet, A., Li, Z., Li, Q., 2022. Adsorption of methylene blue from aqueous solution on activated carbons and composite prepared from an agricultural waste biomass: a comparative study by experimental and advanced modeling analysis. *Chem. Eng. J.* 430, 1385–8947. <https://doi.org/10.1016/j.cej.2021.132801>.
- Yuan, E., Wu, C., Liu, G., Li, G., Wang, L., 2018. Effects of SBA-15 physicochemical properties on performance of Pd/SBA-15 catalysts in 2-ethyl-anthraquinone hydrogenation. *J. Ind. Eng. Chem.* 66, 158–167. <https://doi.org/10.1016/J.JIEC.2018.05.025>.
- Yuan, N., Cai, H., Liu, T., Huang, Q., Zhang, X., 2019a. Adsorptive removal of methylene blue from aqueous solution using coal fly ash-derived mesoporous silica material. *Adsorpt. Sci. Technol.* 37, 333–348. <https://doi.org/10.1177/0263617419827438>.
- Yuan, Q., Yao, B., Huang, Z.R., Huang, Q., 2019b. Developing a liquid and curable two-component precursor system for fabrication of SiC(N)-based composites. *Ceram. Int.* 45, 24007–24013. <https://doi.org/10.1016/J.CERAMINT.2019.08.103>.
- Zhai, Q.-Z., Li, X.-D., 2019. Efficient removal of cadmium(II) with SBA-15 nanoporous silica: studies on equilibrium, isotherm, kinetics and thermodynamics. *Appl. Water Sci.* 2019 96 (9), 1–11. <https://doi.org/10.1007/S13201-019-1022-9>.
- Zhang, J., Ma, Y., Shi, F., Liu, L., Deng, Y., 2009. Room temperature ionic liquids as templates in the synthesis of mesoporous silica via a sol-gel method. *Microporous Mesoporous Mater.* 119, 97–103. <https://doi.org/10.1016/J.MICROMESO.2008.10.003>.
- Zhou, C., Gao, Q., Luo, W., Zhou, Q., Wang, H., Yan, C., Duan, P., 2015. Preparation, characterization and adsorption evaluation of spherical mesoporous Al-MCM-41 from coal fly ash. *J. Taiwan Inst. Chem. Eng. Complete* 147–157. <https://doi.org/10.1016/J.JTICE.2015.02.014>.
- Zhu, J., Wang, Y., Liu, J., Zhang, Y., 2014. Facile one-pot synthesis of novel spherical zeolite-reduced graphene oxide composites for cationic dye adsorption. *Ind. Eng. Chem. Res.* 53, 13711–13717. [https://doi.org/10.1021/IE502030W/ASSET/IMAGES/IE502030W.SOCIAL.JPEG\\_V03](https://doi.org/10.1021/IE502030W/ASSET/IMAGES/IE502030W.SOCIAL.JPEG_V03).